Journal of Translational Medicine

RESEARCH

Open Access

tRNA-derived fragment 3′tRF-AlaAGC modulates cell chemoresistance and M2 macrophage polarization via binding to TRADD in breast cancer

Dongping Mo[1,3†], Xun Tang[1,3†], Yuyan Ma[1,3], Dayu Chen[1], Weiguo Xu[2,3], Ning Jiang[1,3], Junyu Zheng[1] and Feng Yan[1,3*]

Abstract

Background Drug resistance, including Adriamycin-based therapeutic resistance, remains a challenge in breast cancer (BC) treatment. Studies have revealed that macrophages could play a pivotal role in mediating the chemoresistance of cancer cells. Accumulating evidence suggests that tRNA-Derived small RNAs (tDRs) are associated the physiological and pathological processes in multiple cancers. However, the underlying mechanisms of tDRs on chemoresistance of BC in tumor-associated macrophages remain largely unknown.

Methods The high-throughput sequencing technique was used to screen tDRs expression profile in BC cells. Gain- and loss-of-function experiments and xenograft models were performed to verify the biological function of 3′tRF-Ala-AGC in BC cells. The CIBERSORT algorithm was used to investigate immune cell infiltration in BC tissues. To explore the role of 3′tRF-Ala-AGC in macrophages, M2 macrophages transfected with 3′tRF-Ala-AGC mimic or inhibitor were co-cultured with BC cells. Effects on Nuclear factor-κb (NF-κb) pathway were investigated by NF-κb nuclear translocation assay and western blot analysis. RNA pull-down assay was performed to identify 3′tRF-Ala-AGC interacting proteins.

Results A 3′tRF fragment of 3′tRF-AlaAGC was screened, which is significantly overexpressed in BC specimens and Adriamycin-resistant cells. 3′tRF-AlaAGC could promote cell malignant activity and facilitate M2 polarization of macrophages in vitro and in vivo. Higher expression of M2 macrophages were more likely to have lymph node metastasis and deeper invasion in BC patients. Mechanistically, 3′tRF-AlaAGC binds Type 1-associated death domain protein (TRADD) in BC cells, and suppression of TRADD partially abolished the enhanced effect of 3′tRF-AlaAGC mimic on phenotype of M2. The NF-κb signaling pathway was activated in BC cells co-cultured with M2 macrophages transfected with 3′tRF-AlaAGC mimic.

†Dongping Mo and Xun Tang contributed equally to this work.

*Correspondence:
Feng Yan
yanfeng@jszlyy.com.cn

Full list of author information is available at the end of the article

Conclusions 3′tRF-AlaAGC might modulate macrophage polarization via binding to TRADD and increase the effect of M2 on promoting the chemoresistance in BC cells through NF-κb signaling pathway.

Keywords 3′tRF-AlaAGC, TRADD, Macrophages polarization, NF-κb signaling pathway, Chemoresistance, Breast cancer

Introduction

According to the 2020 global new cancer data released by the International Agency for Research on Cancer (IARC) of the World Health Organization, the incidence rate of breast cancer (BC) has surpassed that of lung cancer, becoming the most common cancer [1]. The overall survival of BC patients has obviously improved in the past decades because of the enhancement of comprehensive treatments. However, distal metastasis and drug resistance still lead to poor prognosis. Adriamycin (ADR), is a traditional anthracycline chemotherapeutic drug, which has been widely applied for BC patients as well as other anti-cancer agents due to its ability to break DNA and interfere with transcriptional inhibition of mRNA synthesis, ultimately leading to cell apoptosis [2]. Notwithstanding, ADR destroyed the structure and function of cell membrane, resulting in cytotoxicity and drug resistance, which in turn leads to poor chemotherapy efficacy [3]. Nowadays, drug resistance has become the primary cause of chemotherapy failure, metastasis and recurrence of BC in clinic [4].

Non-coding RNAs (ncRNAs) have been identified and revealed to act as either tumor promoters or antioncogenes in cancer progression. They also play a role in regulating tumor resistant mechanisms, such as long non-coding RNAs in BC [5], microRNAs in melanomas [6], and circular RNAs in gastric cancer [7]. In recent years, a novel ncRNAs named tRNA-Derived small RNAs (tDRs) have gradually attracted researchers' attention, which is derived from specific cleavage of precursor or mature tRNA and expressed in various human cancers [8, 9]. Increasing studies conformed that tDRs perform a variety of valuable functions for the cell, such as involvement in gene silencing, translation efficiency, ribosome genesis, etc., and can regulate tumorigenesis and cancer development at multiple levels [10–12]. A recent study demonstrated that tRF-3024b hijacks miR-192-5p to increase BCL-2-mediated resistance to cytotoxic T lymphocytes in Esophageal Squamous Cell Carcinoma [13], In hormone receptor-positive (HR+) BC, exosome-transmitted tRF-16-K8J7K1B promotes tamoxifen resistance by reducing drug-induced cell apoptosis [14]. Nevertheless, whether tDRs play a pivotal role in Adriamycin resistance in BC remains unclear.

Tumor microenvironment (TME) is a key factor affecting tumor occurrence and progression, which is a local pathological environment composed of tumor cells, endothelial cells, fibroblasts, inflammatory cells and extracellular matrix. In addition, TME provided a favorable environment for drug resistance and immune escape, thereby promoting the growth and metastasis of tumor cells [15, 16]. Macrophages are the most abundant infiltrative immune-related stromal cells present in and around tumors, which transform into M1 and M2 phenotypes with different functions by different stimuli [17]. In BC, M2 type macrophages promote tumor malignant progression, immunosuppression and drug resistance by inducing angiogenesis, degrading tumor extracellular matrix and assisting tumor cells to escape immune surveillance [18–20]. However, the underlying mechanism of M2 macrophages activation in BC drug resistance remains unknown. Recent studies have confirmed that tDRs can exist abundantly and stably in various bodily fluids in the form of free or encapsulated extracellular vesicles, thereby affecting intercellular communication in the TME, while hypoxia, oxidative stress and inflammatory cytokines in the TME can induce or inhibit tDRs [21, 22]. Based on this, we hypothesized that tDRs could affect the phenotype of macrophages in the TME and further regulate the chemoresistance in BC.

In the present study, we identified a specific tDRs (3′tRF-AlaAGC) and explored it's expression pattern and biological function, evaluating whether 3′tRF-AlaAGC could modulate macrophages polarization to affect BC cells chemoresistance. Through in vitro and in vivo experiments, we indicated that 3′tRF-AlaAGC could regulate the phenotype of macrophage via binding to TRADD and increase the effect of M2 macrophage on promoting the chemoresistance in BC cells, hoping that our finding may aid identifying a potential therapeutic target to overcome for drug resistance in BC.

Materials and methods

Clinical samples

The study was approved by the Clinical Research Ethics Committee of Nanjing Medical University (No#2020−130). From 2021 to 2023, we collected 81 serum samples form patients with BC, who visited the thoracic surgery department of Jiangsu Cancer Hospital. All samples were stored at -80℃ after centrifugation until further processing.

Cell culture and cell transfection

The human BC cell lines MCF-7 was obtained from the Cell Bank of Chinese Academy of Sciences (Shanghai, China). The human Adriamycin-resistance cells (MCF-7/

ADR) were purchased from Jiangsu KeyGEN Biotech (KG224) and maintained the drug resistance with 250 ng/ml Adriamycin (KGA8183). The human monocyte cell line THP-1 was obtained from Guangzhou Cellcook Biotech Company (CC1904). THP-1 cells were maintained in RPMI-1640 medium supplemented with 10% (v/v) fetal bovine serum (Gibco Invitrogen, Carlsbad, CA) and 1% antibiotics and 0.05mM β-mercaptoethanol (Aladdin, China) in a 37℃-incubator containing 5% CO2.

Cells were seeded into 6-well or 12-well plates 24 h before transfection and transfected with Lipofectamine™ 3000 transfection reagent (Invitrogen, USA). The synthetic tiRNA single-strand mimic/inhibitor of 3′tRF-Ala-AGC and corresponding negative control (Ribobio, China) were optimized for MCF-7 and MCF-7/ADR cells according to the manufacturer's instructions. Short interfering (si)RNAs targeting TRADD were obtained from Ribobio. There different siRNAs against TRADD were chosen. Cells were transiently transfected with individual siRNAs by using Lipofectamine™ 3000, then collected for subsequent assays after 48 h incubation.

Induction of THP-1 derived macrophages

THP-1 cells were treated with 100 ng/ml phorbol 12-myristate 13-acetate (PMA, MedChemExpress, HY-18,739) for 48 h to generate macrophages as previously reported [17]. The matured macrophages were exposed to LPS (100ng/ml, Solarbio) and IFN-γ (20 ng/ml, PeproTech) for 48 h to obtain M1 polarized macrophage. M2 polarized macrophage were obtained by treatment with IL-4 and IL-13 (20 ng/ml, PeproTech) for 48 h. As for co-culture experiments, macrophage cells were cultured in 0.4 μm pore size 12-well Transwell inserts (LABSELECT, 14,211) while BC cells were cultured in the bottom well of the Transwell chamber.

RNA isolation, cDNA synthesis and quantitative real-time PCR

Total RNA of cells was extracted using TRIzol reagent (Life Technologies, USA). Then, the RNA was quantified using a ribo*SCRIPT*™ Reverse Transcription Kit (Ribobio, China) following the manufacturer's protocol and reverse transcribed to cDNA with Bulge-loop™ miRNA qRT-PCR primers (Ribobio, China) specific for 3′tRF-AlaAGC. SYBR Green Mix was used to perform qPCR in a volume of 10 μl, and 3′tRF-AlaAGC template was normalized to RNU6B. After adding forward primer and reverse primer, the mixtures were incubated at 95 °C for 10 min, followed by 40 cycles at 95 °C for 10 s, 60 °C for 20 s, and 70 °C for 10 s. Other genes were performed with HiScript® II Q RT SuperMix for qPCR (Vazyme, China), β-actin was used for mRNA template normalization. Relative expression levels of 3′tRF-AlaAGC and mRNA were determined via the $2^{-\Delta\Delta CT}$ or $2^{-\Delta CT}$ methods. All primers sequences were shown in Supplementary Table S1.

Gene ontology (GO) and Kyoto encyclopedia of genes and genes and genome (KEGG) pathway enrichment analysis

The GO terms for 3′tRF-AlaAGC target genes based on homologies were extracted (http://www.geneontology.org). The Database for Annotation, Visualization and Integration Discovery software (http://david.abcC.ncifcrf.gov) was used to perform GO analysis to identify biological processes (BP), cellular components (CC), and molecular functions (MF) of these target genes. KEGG database (http://www.genome.jp/kegg/) was used to retrieve 3′tRF-AlaAGC target genes. Go and KEGG analyses with $P<0.05$ were considered as statistically significant.

Adriamycin cytotoxicity assay

For CCK-8 Adriamycin toxicity explorations, cells were plated at a density of $3\text{-}5\times10^3$ cells /well in 96-well. Following 24 h of incubation, serial dilutions of Adriamycin were added to the cells in complete medium for different concentrations. Add an equivalent volume of corresponding vehicle to the wells labeled with drug concentration 0 as the control. While, wells with the reagent combinations but no cells are used as blank. After 24 h of treatment, the medium was replaced by 100 μl of fresh medium and 10 μl CCK-8 reagent (APE×BIO, USA), then incubated for 3–4 h at 37℃. The OD value was measured at 450 nm by microplate reader. Calculate the cell viability of each group according to the following formula: (OD [drug] - OD [blank]) / (OD [control] - OD [blank]) × 100%. For clone formation assay, cells in each group were seeded in 6-well (1×10^3 cells per well) and incubated in complete culture with Adriamycin (3μg/ml) for 7–10 days. At the end of the study, cells were fixed with 4% paraformaldehyde for 15 min at room temperature and stained with 1% crystal violet and the number of clones was counted to assess cell proliferation.

Flow cytometry analysis

M1 and M2 polarized macrophages were harvested and then washed twice in PBS. Cells were resuspended in PBS with a concentration of 1×10^7 cell/ml. A volume of 100 μl of these suspended cells was transferred into flow tubes and stained for 15 min at room temperature with PE Mouse Anti-Human CD86 (BD Pharmingen, 555,665) in the dark. For intracellular staining, add 1×Fix the membrane breaking solution at 4 °C for 25 min according to manufacturer's instructions of Fixation/Permeablization Kit (BD Pharmingen, 554,714). After centrifugation, Alexa Fluor 647 anti-human CD 206 (Biolegend, 321,116) was added and incubated at 4 °C for 30 min. Finally, PBS was resuspended and tested. Prepare single-cell

suspension samples from mice subcutaneous tumor tissue then add PE Anti-CD163 (Abcam 269,322) and Anti-Human CD206 (proteintech 18704-1-AP), Dylight 488, Goat Anti-Rabbit IgG (Abbkine, A23220) as fluorescent secondary antibodies for CD206. After incubation, nucleation, washing, and fixation, flow cytometry was performed.

Cell apoptosis was measured by flow cytometry using Annexin V-FITC/PI kit (Absin, 50001-100T). The transfected cells were harvested after being treated with Adriamycin (3 μg/ml) for 24 h. 500 μl Binding buffer was added to suspension cells. FITC Annexin V (5 μl) and 5 μl propidium iodide (PI) were added and incubated for 5–15 min in the dark according to the manufacturer's protocol. And then, cells were analyzed by Agilent NovoCyte-D2060R. Results were analyzed by NovoExpress software.

Cell cycles were detected using PI/RNase Staining Buffer Kit (BD Pharmingen, 550,825) following the manufacturer's instructions. In short, prepared single cell suspension was fixed with 75% ethanol overnight at 4 ℃ and washed off with PBS before staining. Add 500 μl PI solution for 15 min at room temperature in the dark. DNA content was detected by Agilent NovoCyte-D2060R. The percentage of cells in G1, S and G2 phase was analyzed using NovoExpress software.

In vivo animal model

All animal experimental procedures were approved by the Animal Ethics Committee of the Nanjing Medical University. Eighteen Balb/c nude mice (Female, 4–6 weeks old) were purchased from Hangzhou Ziyuan Experiment Animal Technology Co., Ltd (Hangzhou, China). MCF-7/ADR cells in the logarithmic growth phase were resuspended and digested to a density of 5×10^6 cells/ml. Each mouse was inoculated with 200 μl of cell suspension into the abdominal wall. After the tumor size reached 80 mm^3, mice were randomly divided into three groups. And then, 10 nmol of 3′tRF-AlaAGC agomir and corresponding negative control (NC) were injected into tail vain of the mice every 3 days, for a total of 10 injections. The reagents were purchased from Ribobio (Guangzhou, China), and phosphate buffer saline was injected into the mock group. The weight and tumor diameter of mice were measured every 3 days during administration, and the tumor volume was calculated according to the formula: $width^2\times length\times0.5$. All mice were sacrificed at the end of explorations, and the subcutaneous xenografts tissues in each group were excised and photographed before proceeding with subsequent experiments.

IHC and TUNEL staining

According to the manufacturer's protocol, we performed immunohistochemistry (IHC) assay on the tissue samples. In short, tissue samples were fixed, paraffin-embedded, dewaxed, rehydrated and antigen retrieval. Next, each sample was incubated with primary antibodies overnight at 4℃, followed by incubation with HRP-labeled secondary antibodies at 37 °C for 30 min. Immediately after, sections were incubated with DAB solution and counterstained with hematoxylin and eosin. The staining intensity determined by two pathologists was defined as follows: negative (0); weak (1); moderate (2); strong (3). Images were obtained with a microscope. As for terminal deoxynucleotidyl transferase-mediated dUTP nick end labeling (TUNEL) staining, Sect. (4 μm thick) cut from paraffin-embedded tissue were dewaxed and fixed. And then, repaired with protease K for 20 min at 37 ℃. The TUNEL assay kit (Beyotime Biotechnology, C1088) containing TdT was prepared immediately before use according to the manufacturer's protocol. Subsequent to washing with PBS, the sections were counterstained with DAPI. Images were captured with a fluorescence microscope.

RNA pull-down assay and silver staining

Biotinylated tRF probes were synthesized by RiboBio (Guangzhou, China). RNA pull-down was performed using Pierce™ Magnetic RNA-Protein Pull Down Kit (Thermo, 20,164) according to the manufacturer's instructions. Briefly, Cells lysates prepared in the IP lysis buffer were incubated with biotin-coupled probe of tRFs which was pre-bound on magnetic beads. After incubation at 4 °C for 1–2 h, beads were magnetically separated and washed. Then, washing with the washing buffer, the RNA-bead complexes were harvested using elution buffer and take a boiling water bath for 10 min, and remove the supernatant to obtain the eluent. After pull down assay performed as describe above, supernatant mixed with loading buffer was subjected to SDS-page electrophoresis. Next, we stained and developed the gel until the target band is clear, and then take photos.

Enzyme-linked immunosorbent assay (ELISA)

According to the manufacturer's instructions, the concentration of TGF-β and IL-10 levels were detected with a Human/Mouse/Rat TGF-β1 ELISA Kit (MULTISCIENCES, EK981-96) and Human IL-10 ELISA Kit (MULTISCIENCES, EK110/2–48), respectively.

NF-κb nuclear translocation assay

Effects on NF-κb pathway was detected using the NF-κb Activation Nuclear Translocation Assay Kit (Beyotime, SN368). Cells were fixed and washed with PBS for 3 times. After that, cells were blocked with BSA, and incubated with p65 primary antibody and Cy3 tagged secondary antibody in turns. Finally, DNA staining was performed with 4′,6-diamidino-2-phenylindole (DAPI)

for 5 min at room temperature. Images were acquired by a fluorescence microscope.

Western blot analysis

Total proteins were extracted by RIPA lysate (Servivebio, G2002). Protein concentration determined using a BCA protein assay kit (Servivebio, G2026). Equal amount of protein from each sample were separated by SDS-PAGE and transferred to polyvinylidene fluoride membranes and incubated with primary antibodies directed against target proteins: TNF-α (Servivebio, GB11188), IL-1β (Affinity, AF5103), CD86 (Wanleibio, WL05184), CD206 (Proteintech, 18704-1-AP), IL-10 (Proteintech, 60269-1-Ig for human; Abcam, ab189392 for mice), ABCG2 (Proteintech, 27286-1-AP), MDR1(Proteintech, 22336-1-AP), cleaved-caspase3 (Affinity, AF7022), cleaved-caspase9 (Cell Signaling Technology, 7237T), Bal-2(Affinity, BF9103), TRADD (Proteintech, 15468-1-AP), p65 (Servivebio, GB11997), p-p65 (Servivebio, GB113882), CCL-22(Abcam ab124768). GAPDH (Servivebio, GB15002) and actin (Servivebio, GB15001) chosen as a loading control.

Evaluation and analysis of tumor-infiltrating immune cells

Datasets from Gene Expression Omnibus (GEO, https://www.ncbi.nlm.nih.gov/geo/) was obtained in the public domain, which included expression of different genes and the corresponding clinical information. All gene expression was normalized for further investigations. Finally, we selected GSE25065 as the target dataset, including 56 cases of chemosensitivity and 142 chemoresistance. The GIBERSORT algorithm was used to transform normalized gene expression data into relative proportions of 22 types of immune cells of BC tissues. After screening according to $P<0.05$, 191 samples (55 sensitive tissues vs.136 resistant tissues) from GSE25065 was included for further analysis. The expression of immune cells in was analyzed by R software. A heatmap was used to show the expression pattern of immune cells in chemo-sensitive and chemo-resistant BC tissues.

Statistical analysis

All of the statistical data were conducted using SPSS Statistics Version 20.0 and GraphPad Prism v9.4.1. Data from biological triplicate experiments were presented as mean±standard deviation. Comparisons between two groups were performed using Student's *t*-test or a nonparametric Mann-Whitney *U* test. The Ordinary one-way ANOVA or a nonparametric Kruskal-Wallis test was used to perform statistical analysis of multiple comparison groups of data. $P<0.05$ was accepted as statistically significant.

Results

tDRs are associated with adriamycin resistance in BC

Firstly, the half-maximal inhibitory concentration (IC_{50} value) of MCF-7/ADR and MCF-7 cells were detected by CCK-8 to verify Adriamycin-resistance BC cells. As shown in Fig. 1A, the IC_{50} value of MCF-7/ADR cells was significantly raised (4.28 μg/ml vs. 51.37 μg/ml; $P<0.001$). Compared with MCF-7 cells, the protein level of ABCG2, MDR1 and Bcl-2 in MCF-7/ADR cells increased, while the levels of cleaved-caspase 9 protein decreased (Fig. 1B). All observations indicated that the acquired resistance of BC cells was relatively obvious.

The high-throughput sequencing technique was used to screen tDRs expression profile in MCF-7/ADR and MCF-7 cells. The scatter plot in Fig. 1C indicated that the expression level in the two groups (up- and down-regulated fragments). The identification criteria of differently expressed tDRs were defined as the absolute value of fold change>2 and $P<0.05$. Total 73 novel tDRs, including 39 upregulated and 34 downregulated, were identified (Fig. 1D). According to fold change>2.5, $P<0.05$, with large difference between groups and small difference within groups, 6 up regulation and 4 down regulation tDRs were determined (Fig. 1E). The above 10 tDRs were validated by qRT-PCR, and the results showed that the expression trend of cell line validation was basically consistent with the sequencing results, the expression of tRF-58-75-Ala-AGC-1 (FC=2.066, $P=0.0007$) was significantly upregulated in Adriamycin-resistant cell sublines (Fig. 1F). As shown in Fig. 1G, the novel tRF-58-75-Ala-AGC-1, located at chromosome 6 (chr6:28,763,741−28,763,812) and a length of 72 bp (http://genome.ucsc.edu/). In the MINTbase v2.0 (http://cm.jefferson.edu/MINTbase/.), the molecule of tRF-58-75-Ala-AGC-1 belong to a class of 18nt small RNAs and the sequence is 5′-TCCCCAGTACCTCCACCA-3′. The fragments matched perfectly to the 3′ end of mature tRNA- Ala-AGC-1-1 and cleavage site is located on the T-loop in the sequence. Figure 1H displayed dissolution curve and amplification curve of tRF-58-75-Ala-AGC-1 in BC cells using qRT-PCR. Subsequently, we performed the Sanger sequencing of the PCR products, and the sequences matched perfectly (Fig. 1I). Finally, we further detected the expression of tRF-58-75-Ala-AGC-1 in serum from 81 BC patients. As shown in Fig. 1J, higher expression of tRF-58-75-Ala-AGC-1 was observed in patients with higher T stages (T1 vs. T3-4: $P=0.0036$; T2 vs. T3-4: $P=0.0314$) and lymph node metastasis ($P=0.0117$). Furthermore, when all BC serum samples were segregated based upon TNM stage, the gradual increase in serum tRF-58-75-Ala-AGC-1 expression levels was clearly discernible ($P=0.0001$). According to the naming method of *Tao* et al. [23], we named tRF-58-75-Ala-AGC-1 as 3′tRF-AlaAGC.

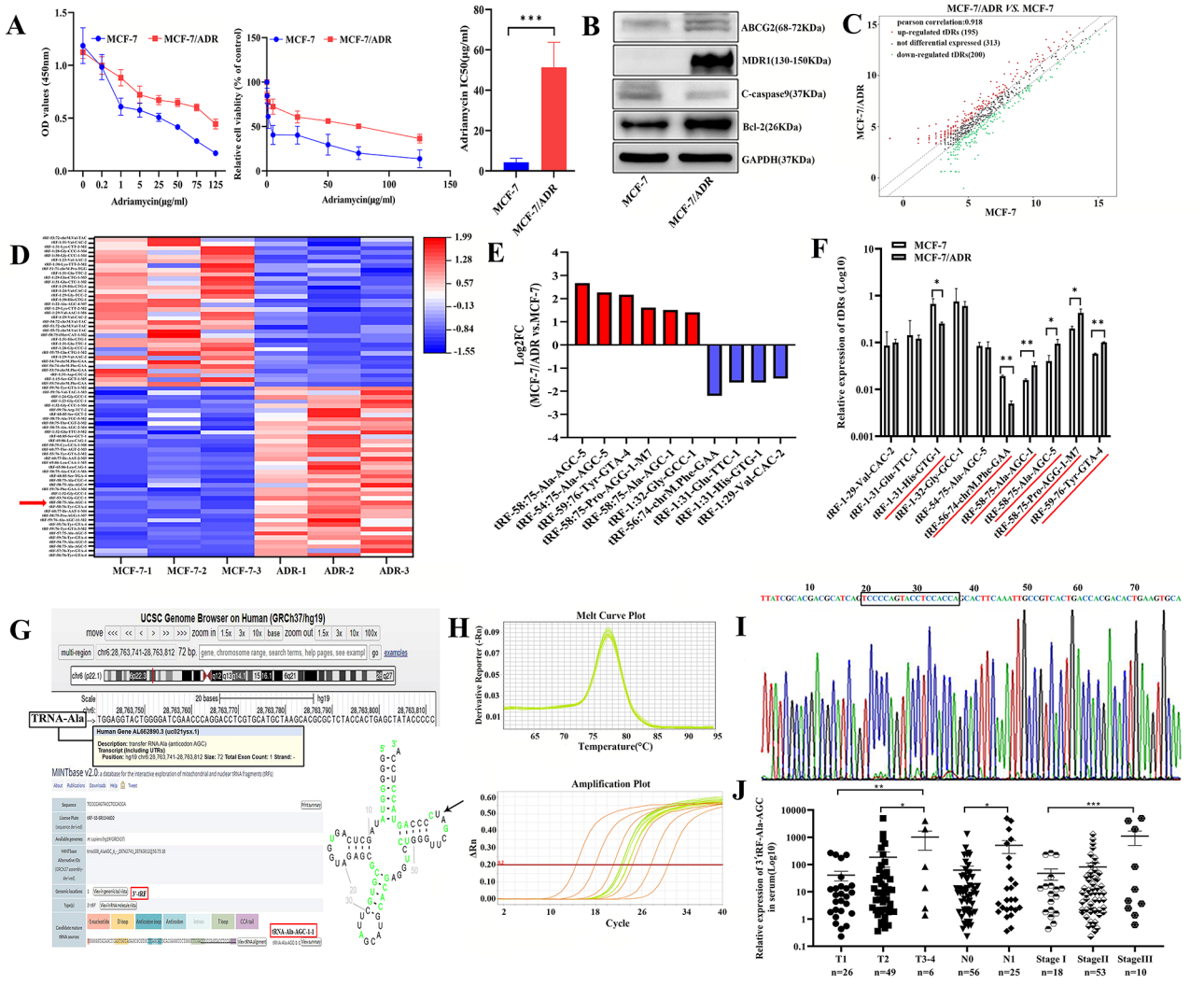

Fig. 1 tDRs are associated with Adriamycin resistance in breast cancer. **A** The CCK-8 toxicity confirming the IC_{50} value in MCF-7 and MCF-7/ADR cells. **B** Western blot analysis for ABCG2, MDR1, cleaved caspase-9 and Bcl-2 in breast cancer cells. **C** The scatter plot between two groups for tDRs. **D** The heatmap of 73 candidate tumor-related differential tDRs. **E** Ten tDRs between the two groups, of which 6 were up-regulated and 4 were down-regulated in MCF-7/ADR cells. **F** RT-PCR was used to verify 10 different tDRs in two cell lines. **G** The biological characteristics of tRF-58-75-Ala-AGC-1 in UCSC and MINTbase database. **H** Dissolution curve and amplification curve of tRF-58-75-Ala-AGC-1. **I** The product of qRT-PCR was confirmed by Sanger sequencing. **J** Scatter plot representation of tRF-58-75-Ala-AGC-1 level in serum of breast cancer patients. $^{*}P < 0.05$, $^{**}P < 0.01$

3′ tRF-AlaAGC suppressed chemosensitivity of BC

The relative high expression cell line MCF-7/ADR and relative low expression cell line MCF-7 were selected to inhibition or overexpression 3′tRF-AlaAGC, respectively. MCF-7/ADR cells with 3′tRF-AlaAGC inhibitor performed higher Adriamycin toxicity and lower viability compared with the negative control (Fig. 2A). Colony formation assay displayed that 3′tRF-AlaAGC inhibitor significantly decreased the number of cell clone (Fig. 2B). Meanwhile, flow cytometry analysis showed that inhibition of 3′tRF-AlaAGC significantly increased the percentage of cells in the G1 peak and the apoptosis ability in MCF-7/ADR cell (Fig. 2C, D). In contrast, 3′tRF-AlaAGC mimic showed the opposite tendency in MCF-7 cell (Fig. 2E-H). Taken together, these finding suggested that 3′tRF-AlaAGC promoted BC cells Adriamycin resistance in vitro.

Subcutaneous xenograft experiments were undertaken to discuss the function of 3′tRF-AlaAGC in vivo. As shown in Fig. 2I, the bodyweight of the nude mice in 3′tRF-AlaAGC agomir group markedly decreased compared with the control group. But then, the volume and weight of subcutaneous tumors were significantly enhanced in 3′tRF-AlaAGC agomir group relative to that of the control group (Fig. 2J). The results of western blot assays revealed that the level of cleaved caspase-3 and cleaved caspase-9 in 3′tRF-AlaAGC agomir group decreased, while the levels of Bcl-2 increased (Fig. 2K).

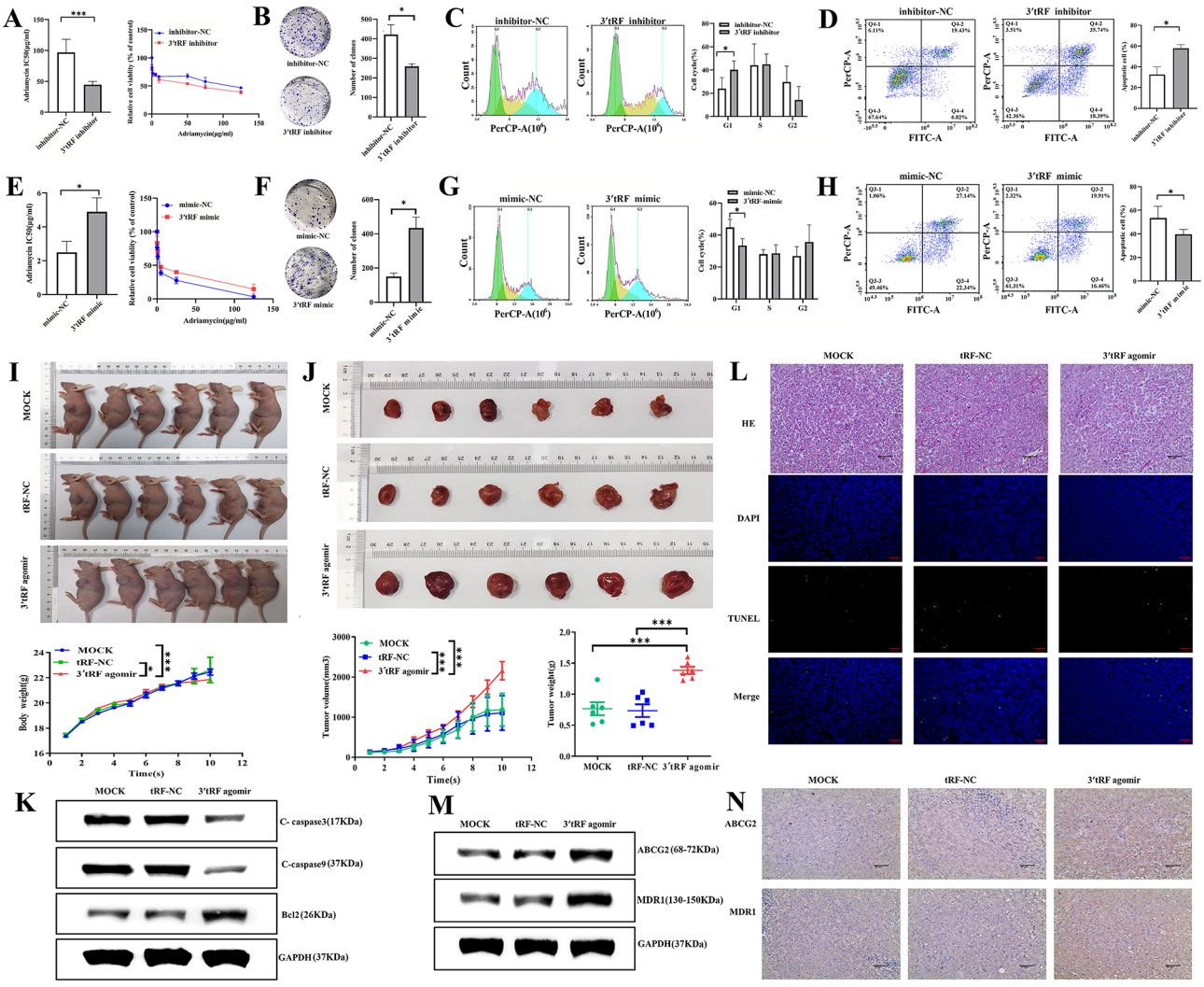

Fig. 2 3′tRF-AlaAGC suppressed chemosensitivity of breast cancer. **A** The CCK-8 toxicity confirming the IC_{50} value in MCF-7/ADR cells transfected 3′tRF-AlaAGC inhibitor. **B** Colony formation assays in cells transfected 3′tRF-AlaAGC inhibitor. **C**, **D** The flow cytometry assays were performed to detected the cell cycle and cell apoptosis ability. **E-H** The cell function assays in MCF-7 cells transfected 3′tRF-AlaAGC mimic. **I** Images of MCF-7/ADR xenografts in vivo and quantification of bodyweight of nude mice. **J** Images of excised tumors from mice after the 10th injection of the reagent and quantification of xenografts tumor volume and weight. **K** The western blot assay detected the level of cleaved caspase-3, cleaved caspase-9 and Bcl-2. **L** Tumor tissue slices were stained with hematoxylin-eosin and TUNEL assay in the three groups. **M**, **N** Western blot analysis and immunohistochemistry demonstrated the level of ABCG2 and MDR1. *$P < 0.05$, **$P < 0.01$, ***$P < 0.001$. 3′ tRF: 3′ tRF-AlaAGC

Moreover, the TUNEL assay displayed that 3′tRF-AlaAGC suppressed the apoptosis of the tumor cells of transplanted mice (Fig. 2L). Besides, the western blot assays and IHC assays demonstrated the high expression of ABCG2 and MDR1 in the 3′tRF-AlaAGC agomir group (Fig. 2M, N). These results indicated that 3′tRF-AlaAGC weakened chemosensitivity of BC in vivo.

The landscape of immune infiltration in BC tissue

We investigated the expression of different immune cells in BC tissues according to the CIBERSORT algorithm. As shown in Fig. 3A, the expression of 22 subpopulations of immune cells varies significantly between chemo-sensitive and chemo-resistant BC tissues (55 sensitive tissues vs.136 resistant tissues). In the heatmap, there were greater differences in the expression of M0, M1 and M2 macrophage between the chemo-sensitive and chemo-resistant tissues among the immune cells (Fig. 3B). It suggested that macrophages with different phenotypes maybe play a key role in mediating drug resistance in BC. Violin diagram was used to analyze the differential expression of 22 immune cells in the two groups. Compared with chemo-sensitive BC tissues, the relative expression of M2 macrophages in chemo-resistant tissues tended to increase (Fig. 3C, $P=0.11$). Nevertheless, Fig. 3D analyzes the correlation of different

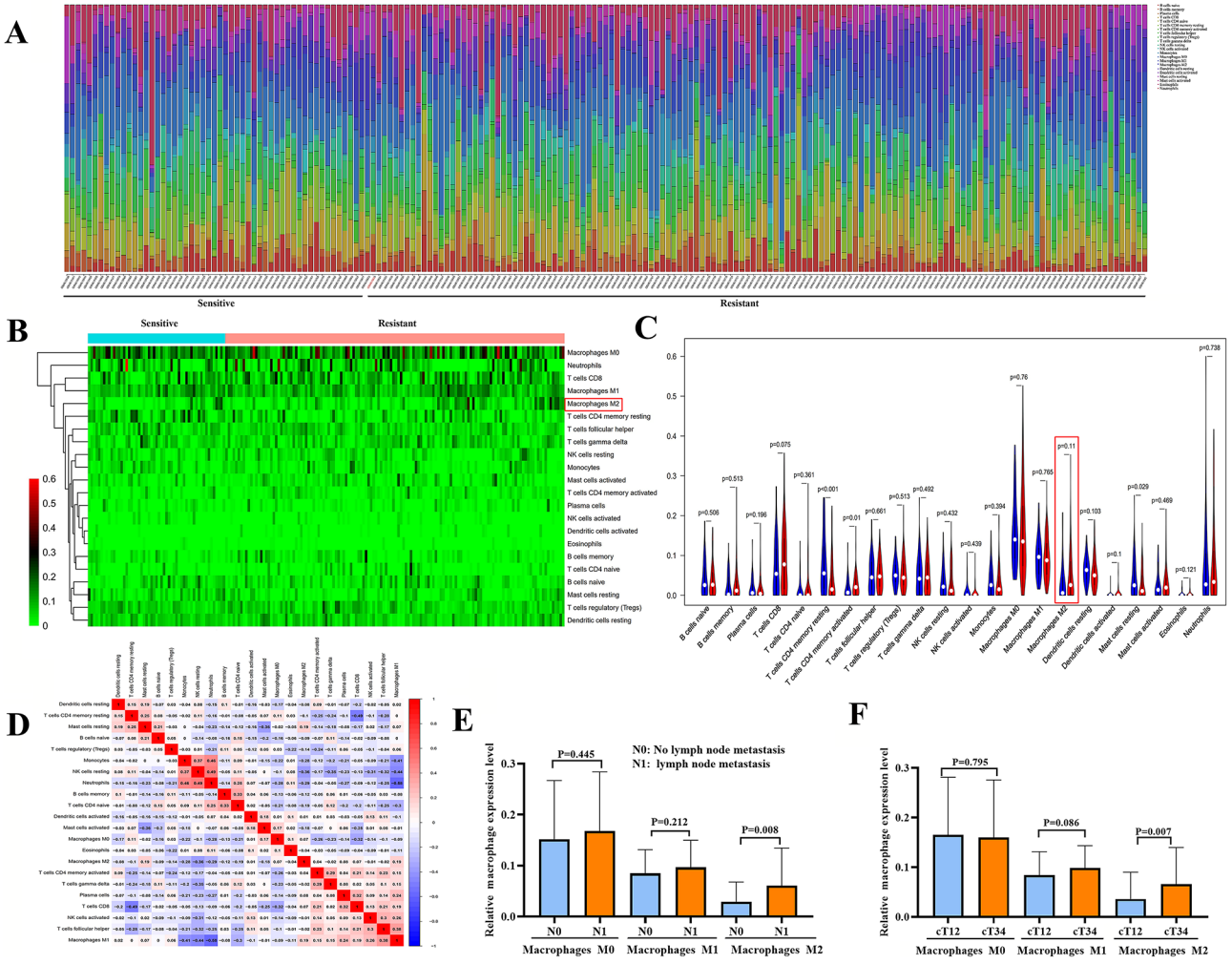

Fig. 3 The landscape of immune infiltration in breast cancer tissues. **A** The histogram shows the relative expression of 22 subpopulations of immune cells in each tissue sample. **B** The heatmap reveals the differential expression of different immune cells in sensitive and resistant tissues. **C** Violin diagram was used to analyze the expression difference of 22 subpopulations of immune cells in the two groups. **D** Correlation heat map shows the correlation analysis of immune cells. **E** The relationship between the relative expression of macrophages with different phenotypes and lymph node metastasis of breast cancer. **F** The relationship between the relative expression of macrophages and the clinical stage of breast cancer

immune cells in BC tissue. The results displayed that the expression of M2 macrophages was negatively correlated with NK cells resting. Finally, we further analyzed the correlation between M2 macrophages and pathological parameters in chemo-resistant BC tissues according to the GSE25065 dataset. Results displayed that those with higher expression of M2 macrophages were more likely to have lymph node metastasis (P=0.008, Fig. 3E) and deeper invasion (cT12 vs. cT34: P=0.007, Fig. 3F).

M2 macrophages promoted the chemoresistance of BC

Human THP-1 monocyte cells were treated with PMA to generate macrophages. M0 macrophages were then polarized toward M1 and M2 with LPS/IFN-γ and IL-4/IL-13, respectively. The growth state of THP-1 cells has changed from the original suspended state to adherent state, and the cells have grown into pseudopods (Fig. 4A). By measuring the mRNA levels of macrophages, M1-polarized macrophage exhibited significantly higher expressions of IL-1β, TNF-α and CD86 than the M0 and M2 macrophages. While compared with M0 and M1 macrophages, the expression of CCL22, IL-10 and CD206 were markedly higher in M2 macrophages (Fig. 4B). Similar results were also reflected in western blot assay, that is, IL-1β, CD86 and TNF-α were highly expressed in M1 macrophages than M0 and M2 macrophages. In contrast, M2 macrophages were shown to highly express CD206 and IL-10 (Fig. 4C). Furthermore, flow cytometry showed that CD86 expression was higher in M1 macrophages, and CD206 was higher in M2 macrophages (Fig. 4D). The co-culture system of BC cells and macrophages is presented in Fig. 4E.

Subsequently, MCF-7 and MCF-7/ADR cells were co-cultured with M0, M1 and M2 macrophages to

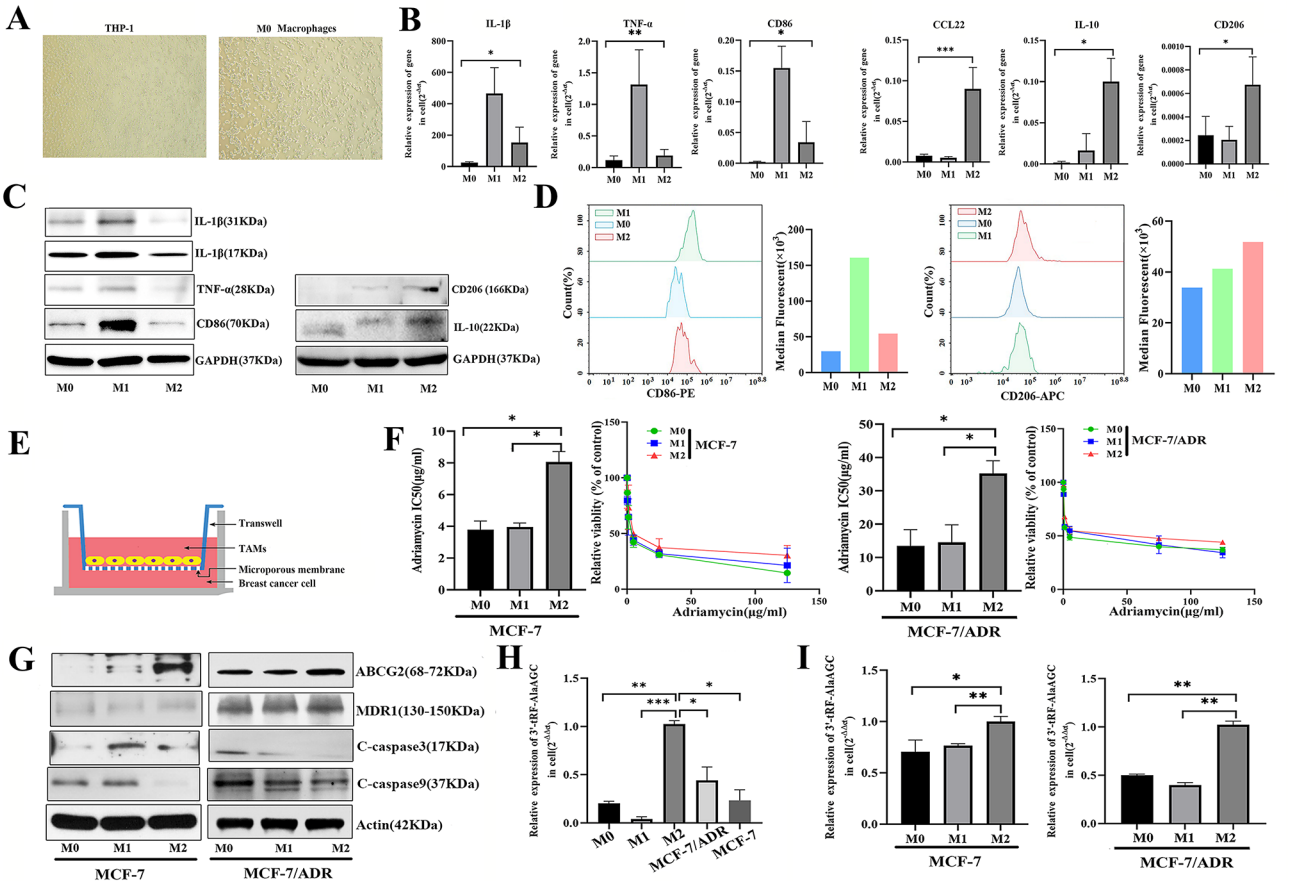

Fig. 4 M2 macrophages promoted the chemoresistance of breast cancer. **A** Representative image (200×) of morphology in THP-1 cells and macrophages. **B** RT-PCR detection of IL-1β, TNF-α, CD86, CCL22, IL-10 and CD206 mRNA expression in M0, M1 and M2 macrophages. **C** Western blot assay analyzed the protein level of IL-1β, TNF-α, CD86, CD206 and IL-10 in macrophages. **D** Flow cytometry detected the markers of M1 macrophages (CD86) and M2 macrophages (CD206). **E** Schematic diagram of co-culture of breast cancer cells and macrophages. **F** CCK8 assay was used to detect the viability of MCF-7 and MCF-7/ADR cells co-culture with macrophages. **G** The protein levels of ABCG2, MDR1, cleaved caspase-3 and cleaved caspase-9 in MCF-7 and MCF-7/ADR cells co-cultured with macrophages. **H** The expression level of 3′tRF-AlaAGC in macrophages and breast cancer cells. **I** The expression level of 3′tRF-AlaAGC in MCF-7 and MCF-7/ADR cells co-cultured with macrophages. **P* < 0.05, ***P* < 0.01, ****P* < 0.001. TAM: Tumor associated macrophages, M0: M0 macrophages, M1: M1 macrophages, M2: M2 macrophages

investigate the influence of distinct macrophage phenotypes on BC cells. As showed in Fig. 4F, MCF-7 and MCF-7/ADR cells were co-cultured with M0, M1 and M2 macrophages, then exposed to Adriamycin for 24 h. The IC50 value of BC cells co-culture with M2 macrophages was significantly higher than that of cells co-culture with M0 and M1 macrophages. In a word, M2 macrophages could enhance the chemoresistance of BC cells. Moreover, the higher protein level of MDR1, ABCG2 and lower protein level of cleaved caspase-3, cleaved caspase-9 in BC cells co-culture with M2 macrophages (Fig. 4G).

Finally, the expression of 3′tRF-AlaAGC in M0, M1, M2 macrophages and BC cell was detected with real-time PCR. The 3′tRF-AlaAGC expression level in M2 macrophages was significantly higher than other cells (Fig. 4H). In addition, the 3′tRF-AlaAGC expression level in BC cells co-culture with M2 macrophages was also markedly higher than that of cells co-culture with M0 and M1 macrophages (Fig. 4I). These results suggested that increased expression of 3′tRF-AlaAGC in M2 macrophages may be involved in regulating the effect of macrophages on drug resistance of BC cells.

M2 macrophages treated with 3′tRF-AlaAGC regulated chemoresistance of BC cells

In order to investigate the role of 3′tRF-AlaAGC in M2 macrophages, we transfected 3′tRF-AlaAGC inhibitor or mimic into M2 macrophages and co-cultured them with BC cells. MCF-7/ADR cells co-cultured with M2 macrophages transfected with 3′tRF-AlaAGC inhibitor exhibited reduced drug resistance, halted cell cycle progression, and increased apoptosis (Fig. 5A-C). Moreover, there were lower expression of ABCG2, Bcl-2 and higher expression of cleaved caspase-3, cleaved caspase-9 compared with negative group (Fig. 5D). In contrast, the

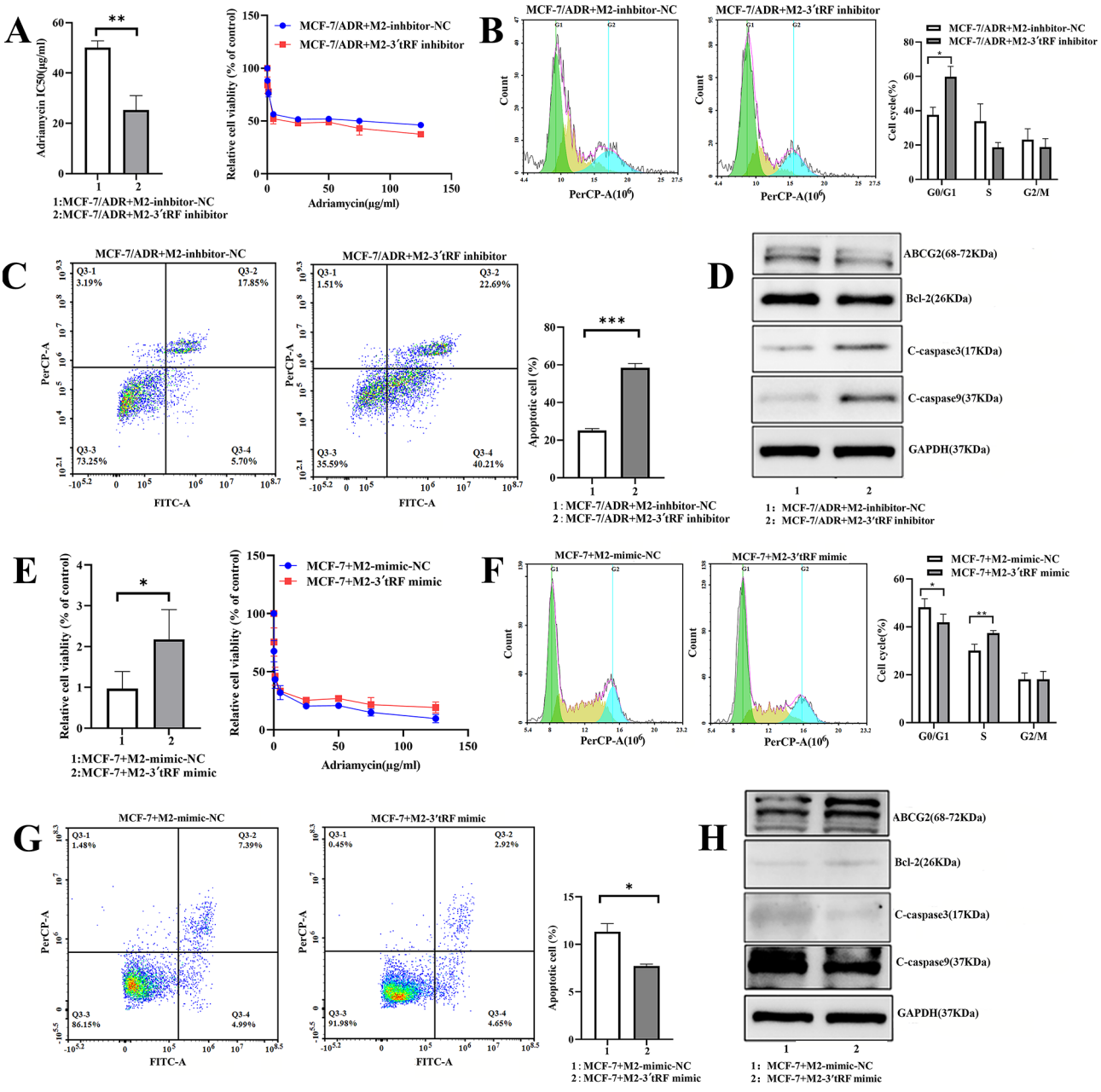

Fig. 5 M2 macrophages treated with 3′tRF-AlaAGC regulated chemoresistance of breast cancer cells. **A** The CCK-8 toxicity confirming the IC_{50} value in MCF-7/ADR cells co-cultured with M2 macrophages transfected with 3′tRF-AlaAGC inhibitor. **B**, **C** The flow cytometry assays were performed to detected the cell cycle and cell apoptosis ability in MCF-7/ADR cells co-cultured with M2 macrophages transfected with 3′tRF-AlaAGC inhibitor. **D** Western blot assay analyzed the protein level. **E-H** The cell function assays in MCF-7 cells co-cultured with M2 macrophages transfected with 3′tRF-AlaAGC mimic. $^{*}P < 0.05$, $^{**}P < 0.01$, $^{***}P < 0.001$. 3′ tRF: 3′ tRF-Ala-AGC, M2: M2 macrophages

MCF-7 cells co-cultured with the M2 macrophages transfected with 3′tRF-AlaAGC mimic showed the opposite tendency, that is, attenuated chemosensitivity (Fig. 5E-H). The above results suggested that 3′tRF-AlaAGC in the M2 macrophages could regulate the chemotherapy effect of BC cells.

3′tRF-AlaAGC induces M2 polarization of macrophage

We transfected the 3′tRF-AlaAGC mimic/inhibitor and negative control into M1 and M2 macrophages, respectively. Interestingly, we found that after transfection with 3′tRF-AlaAGC mimic, the expression of IL-10 and CCL22 (markers of M2 macrophages) in macrophages increased significantly, while the expression of TNF-α and IL-1β (markers of M1 macrophages) decreased. Conversely, after transfection with inhibitor, the expression

of IL-10 and CCL22 in macrophages decreased, and the expression of TNF-α and IL-1β increased (Fig. 6A). Meanwhile, the ELISA results also demonstrated that the levels of TGF-β and IL-10 in supernatant of M1 and M2 macrophages treated with 3′tRF-AlaAGC mimic were higher than those in control cells. As for the cells transfected with inhibitor, the concentrations of TGF-β and IL-10 in supernatant were relatively low (Fig. 6B).

In the subcutaneous tumor tissue of mice, the mRNA and protein levels of IL-10 and CCL22 were significantly increased in the 3′tRF-AlaAGC agomir group compared with the control groups (Fig. 6C, E). In addition, the concentrations of TGF-β and IL-10 in mice serum of 3′tRF-AlaAGC agomir group were markedly raised (Fig. 6D). Flow cytometry results revealed that $CD206^{+}CD163^{+}$ expression in the 3′tRF-AlaAGC agomir group was significantly increased compared with the control groups (Fig. 6F). Based on the above results, we inferred that 3′tRF-AlaAGC could regulate the phenotype of macrophages.

M2 macrophages treated with 3′tRF-AlaAGC regulate chemoresistance of BC cells through NF-κb signaling

According to the data of GSE25065, 198 BC tissues divided into drug resistant group and sensitive group, and the differential expression signals were analyzed by GESA software (http://www.webgestalt.org/). As shown in Fig. 7A, the expression of NK-κb signaling pathway in drug resistant group was enhanced. The results of GO analysis of the DEGs-3′tRF-AlaAGC target genes were presented in Fig. 7B, which revealed that these target genes were significantly enriched in BP of regulation of signaling, positive regulation of cellular process and generation of neurons. The significant CC terms included intracellular, cytoplasm, cell junction and organelle membrane. MF terms included protein binding, enzyme binding and transcription regulator activity. Meanwhile, enriched signaling pathways for target genes of 3′tRF-AlaAGC identified by KEGG pathway analysis were ranked according to the $-\log_{10}$(pvalue). The significant 14 signaling pathway include Ras signaling pathway, cAMP signaling pathway, Cell adhesion molecules, TNF signaling pathway, NF-κb signaling pathway and so on in MCF-7 and MCF-7/ADR cells (Fig. 7C). The above results suggesting that NF-κb signaling pathway may be

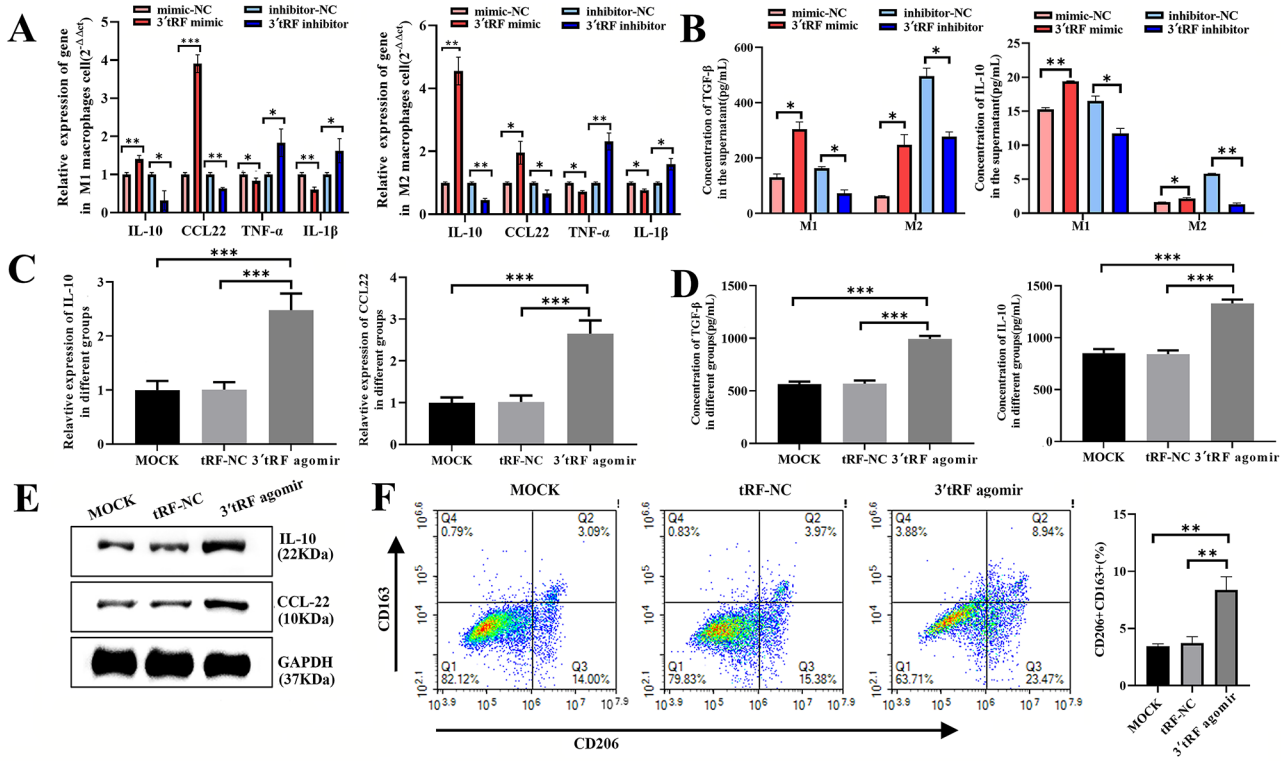

Fig. 6 3′ tRF induced M2 polarization of macrophages **A** Real-time PCR detection of IL-10, CCL22, TNF-α and IL-1β expression in M1 and M2 macrophages transfected with 3′tRF-Ala-AGC mimic or inhibitor, U6 were used as the control. **B** The concentration of TGF-β and IL-10 in supernatants of M1 and M2 transfected with 3′tRF-AlaAGC mimic or inhibitor. **C** The mRNA levels of IL-10 and CCL22 in the subcutaneous tumor tissue of mice. **D** The concentration of TGF-β and IL-10 in mice serum. **E** The protein levels of IL-10 and CCL22 in the subcutaneous tumor tissue of mice. **F** Flow cytometry was used to quantify the expression of CD206 and CD163. *$P < 0.05$, **$P < 0.01$, ***$P < 0.001$. 3′ tRF: 3′ tRF-Ala-AGC, M1: M1 macrophages, M2: M2 macrophages

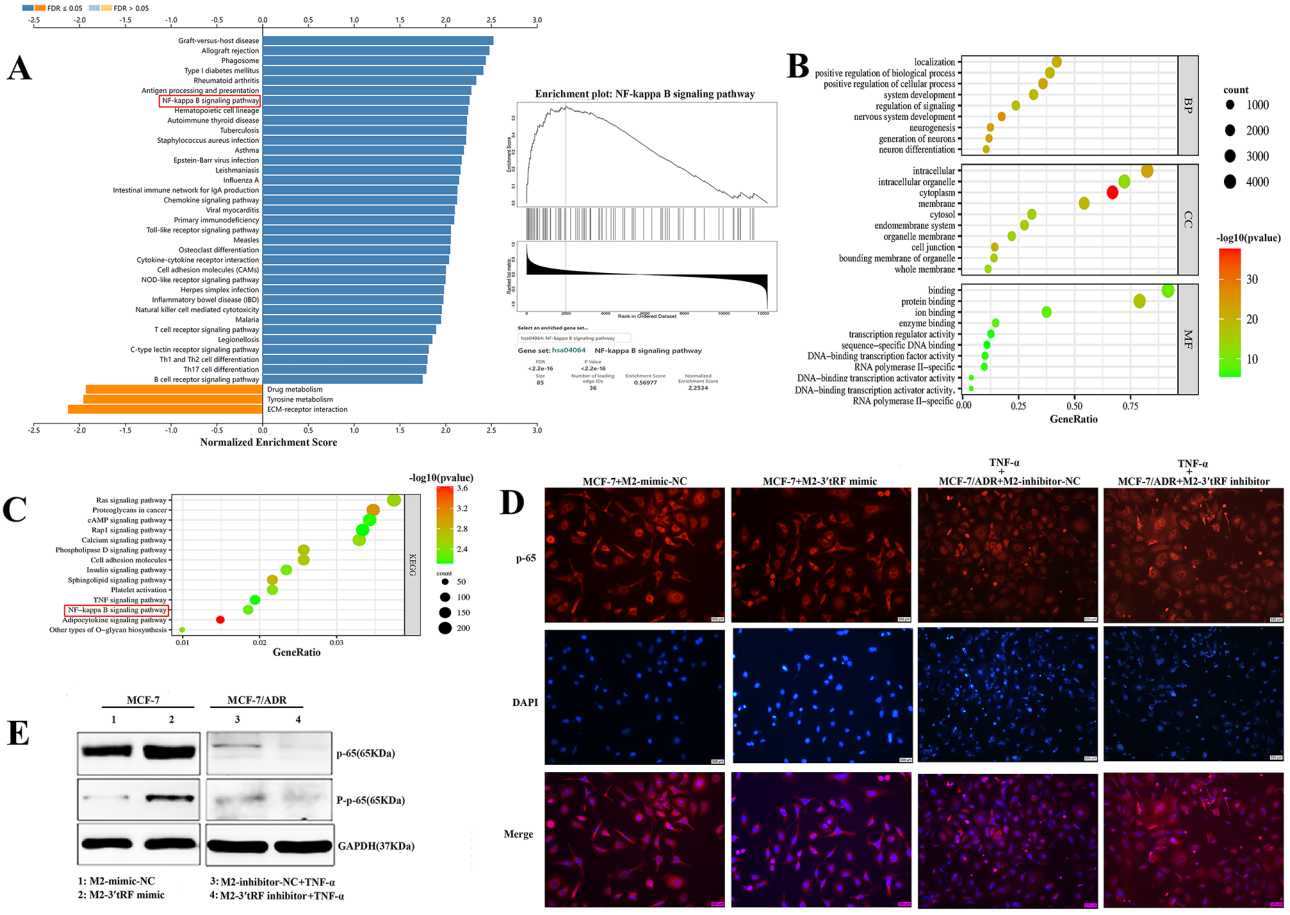

Fig. 7 M2 macrophages treated with 3′tRF-AlaAGC regulated chemoresistance of breast cancer cells through NF-κb signaling. **A** GSEA Analysis of differential Expression of NF-κb pathway signal in drug resistant and sensitive breast cancer tissues. **B** GO analysis of the DEGs-3′-tRF-AlaAGC target genes. **C** KEGG pathway analysis showed that the 14 related pathways changed significant in breast cancer cells. **D** Effects on NF-κb pathway was detected using the NF-κb Activation Nuclear Translocation Assay Kit. **E** Western blot assay analyzed the protein level of p-65 and P-p-65. 3′ tRF: 3′ tRF-AlaAGC, M2: M2 macrophages

involved in the regulation of drug resistance in BC. NF-κb family transcription factors are key conditioning factors for immune response, inflammation and cancer, and participate in the regulation of cell apoptosis through various mechanisms [24]. Subsequently, we investigated the influences of BC cells co-cultured with M2 macrophages transfected with 3′tRF-AlaAGC mimic or inhibitor on NF-κb signaling pathway by NF-κb nuclear translocation assay and western blot analysis. Nuclear translocation of p65 was observed after 24 h of MCF-7 cell co-cultured with M2 macrophages transfected with 3′tRF-AlaAGC mimic, which confirmed the activation of NF-κb signaling. And the translocation of p65 elicited by HumanKine® recombinant human TNF-α protein (proteintech, HZ-1014-10UG) with a concentration of 10ng/ml was distinctly suppressed of MCF-7/ADR cell co-cultured with M2 macrophages transfected with 3′tRF-AlaAGC inhibitor (Fig. 7D). Western blot results displayed that MCF-7 cells co-cultured with M2 macrophages transfected with mimic significantly increased the expression of p-65 and P-p-65. Conversely, MCF-7/ADR cells co-cultured with M2 macrophages transfected with inhibitor showed a decrease in the expression of p-65 and P-p-65 (Fig. 7E). Therefore, these results revealed that 3′tRF-AlaAGC in M2 macrophages regulate the chemoresistance BC cells via NF-κb signaling pathway.

3′tRF-AlaAGC regulated M2 polarization of macrophages in a TRADD-mediated manner

TRADD is an adaptor molecule involved in mediating multiple biological activities, including cell survival, cell proliferation, cell differentiation, apoptosis, necroptosis and inflammation. It has a variety of protein binding partners and participates in different signal pathways, including NF-κb and Mitogen Activated Protein Kinase activation [25, 26]. To validate the expression correlation between TRADD and NF-κb, we used TCGA data to preform co-expression analyses via GEPIA (Gene Expression Profiling Interactive Analysis; http://gepia.cancer-pku.cn/index.html). TRADD expression was

positively associated with NF-κb ($r=0.3$, $P<0.01$) in BC (Fig. 8A). What's more, the results of qRT-PCR and western blot analysis showed that down-regulation of 3′tRF-AlaAGC induced a significant decrease of TRADD in MCF-7/ADR cells. In contrast, in MCF-7 cells transfected with mimic showed the opposite tendency (Fig. 8B). Then, the statistical analysis in public databases TCGA revealed that the level of TRADD in BC was significantly higher than normal samples (Fig. 8C, $P<0.001$). In addition, compared with chemo-sensitive BC tissues, the relative expression of TRADD was significantly higher in chemo-resistant tissues (Fig. 8D, $P=0.035$). Interestingly, analysis of the TRADD 3′-UTR sequence using TargetScan (http://www.targetscan.org/) and microRNA.org (http://www.microrna.org/microrna/) revealed the possible binding site for 3′tRF-AlaAGC, implying that the TRADD gene transcript may be a direct target of 3′tRF-AlaAGC (Fig. 8E). After that, we performed RNA pull-down assay and silver staining assay to detect 3′tRF-AlaAGC-associated proteins (Fig. 8F, G). Indeed, the results evidenced that the association of 3′tRF-AlaAGC with TRADD.

To determine whether the dysregulation of TRADD is involved in the regulate the phenotype of macrophages by 3′tRF-AlaAGC, we used specific siRNAs against TRADD to knock down TRADD expression and verified that si-TRADD-2 have relatively high knockdown efficiency for MCF-7 and MCF-7/ADR cells (55% and

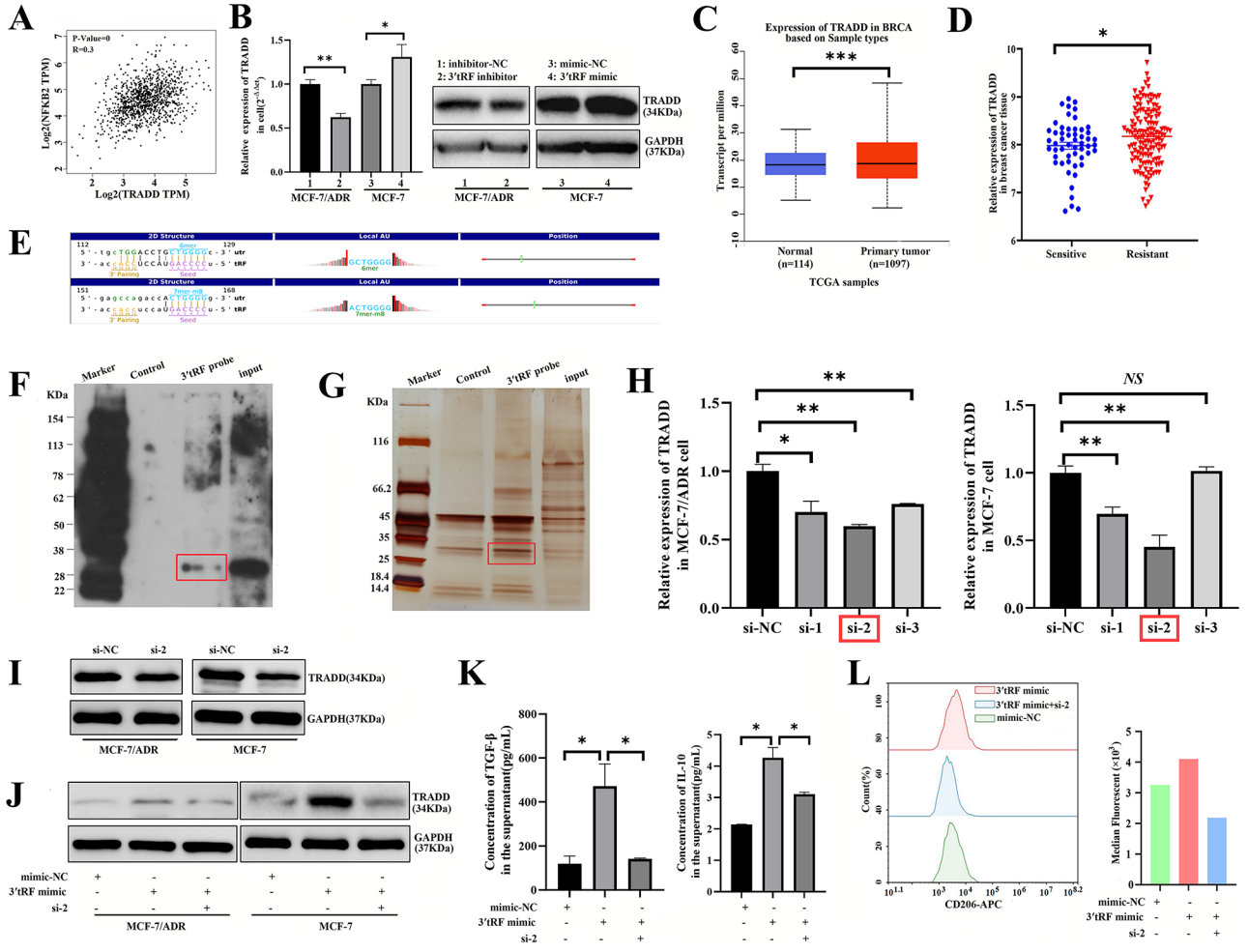

Fig. 8 3′tRF-AlaAGC regulated M2 polarization of macrophages in a TRADD-mediated manner. **A** The expression correlation of TRADD and NF-κb in clinical breast cancer specimens. **B** The mRNA and protein expression level of TRADD in cells transfected with 3′tRF-AlaAGC inhibitor or mimic. **C** The levels of TRADD between cancer and normal samples in TCGA database. **D** The levels of TRADD between chemo-sensitive and chemo-resistant tissues. **E** The 3′UTR area of TRADD combined with 3′tRF-AlaAGC. **F** Western blot analysis of products from RNA pull-down assays using the 3′tRF-AlaAGC probe suggested TRADD in MCF-7/ADR cells. **G** Silver SDS-PAGE gel image shows proteins immunoprecipitated by the 3′tRF-AlaAGC probe in MCF-7/ADR cells. **H** The mRNA expression levels of TRADD in cells transfected with TRADD siRNA. **I** Protein levels in cells transfected with si-TRADD and negative control. **J** Western blot analysis was used to detect TRADD expression in cells transfected with 3′tRF-AlaAGC, si-TARDD or negative control. **K** The amounts of TGF-β and IL-10 in the supernatants of 3′tRF-AlaAGC mimic and si-TRADD co-transfected M2 macrophages determined by ELISA. **L** The level of CD206 was detected by flow cytometry. *$P<0.05$, **$P<0.01$, ***$P<0.001$. 3′ tRF: 3′ tRF-AlaAGC, si-2: si-TRADD-2

41%, respectively; Fig. 8H, I). As shown in Fig. 8J, co-transfected with TRADD siRNA significantly eliminated the elevated protein expression of TRADD induced by the 3′tRF-AlaAGC mimic in BC cells. Moreover, the level of TGF-β and IL-10 in the supernatant of 3′tRF-AlaAGC mimic and si-TRADD co-transfected M2 macrophages was lower than that in cells transfected with mimic alone (Fig. 8K). Furthermore, flow cytometry showed that the level of CD206 was partially attenuated after 3′tRF-AlaAGC mimic and si-TRADD co-stimulation (Fig. 8L). These data illustrated that 3′tRF-AlaAGC regulates M2 polarization of macrophages in a TRADD-mediated manner.

Discussion

Over the past decades, the overall prognosis of patients with early-stage BC has been greatly improved through standard chemotherapy after surgical resection. Anthracycline drugs, such as Adriamycin, as first-line chemotherapy drugs for BC, which inhibit DNA synthesis and cause cell apoptosis. However, chemotherapy is not effective due to drug resistance. Nowadays, with the development of sequencing technology, new types of small non-coding RNAs including tDRs have been identified in kinds of cancer [27, 28]. Accumulating evidence showed that tDRs can be involved in drug resistance of multiple tumors [29]. tDRs can replace the eukaryotic translation initiation factor 4G (eIF4G) that binds to mRNA, thereby inhibiting protein translation [30]. In addition, they can promote the distribution of stress granules (SGs) associated with drug resistance under stress conditions [31, 32]. In the current study, our data displayed that 3′tRF-AlaAGC was markedly upregulated in Adriamycin resistant BC cell. Higher expression of 3′tRF-AlaAGC were more likely to have lymph node metastasis and deeper invasion in patients with BC. Meanwhile, gain- and loss-of-function experiments of 3′tRF-AlaAGC in BC cells demonstrated that 3′tRF-AlaAGC could promote cell Adriamycin resistance and the progression of cell cycle, and suppress cell apoptosis. Consistent with the result, the animal experiments suggested 3′tRF-AlaAGC weakened chemosensitivity of BC in vivo.

Increasing evidence indicated that the acquired resistance could be induced by the TME [16, 33]. Tumor associated macrophage (TAMs) is an important part of TME, which number and phenotype of macrophages are closely related to tumor growth and prognosis [34–36]. The M2 macrophages can play an immunosuppressive and tumorigenic role as TAMs. In this study, we found that expression of M2 macrophages correlated with the cTNM stage and lymph node metastasis of BC. Compared with M0 and M1 macrophages, M2 macrophages could enhance the chemoresistance of BC cells and suppress cell apoptosis. Furthermore, M2 macrophages is highly expressed 3′tRF-AlaAGC, and 3′tRF-AlaAGC level in BC cells co-culture with M2 macrophages was also significantly higher than that of cells co-culture with M0 and M1 macrophages. Importantly, the 3′tRF-AlaAGC in M2 macrophages might impact the chemoresistance of BC cells by regulating the polarization of M2 macrophages.

Macrophages display a high plasticity, which allows them to adapt their phenotype in response to different environmental stimuli [37]. Many studies have shown that macrophages predominantly exhibit a M2-like phenotype in malignant tumors [38]. Tumor associated M2 macrophages improve tumor cell growth and survival and stimulate angiogenesis and metastases. In recent years, several studies have revealed that non-coding RNAs can regulate the polarization of macrophages. For instance, miR-934 induced M2 macrophage polarization by downregulating PTEN expression and activating the PI3K/AKT signaling pathway in colorectal cancer [39]. LncRNA MIR155HG promotes colorectal cancer progression and enhances oxaliplatin resistance in CRC cells through M2 macrophage polarization by regulating ANXA2 [36]. tsRNA-14,783 might be participated in keloid formation via regulation of M2 macrophages polarization [40]. The results of our study indicated that BC cells co-cultured with M2 macrophages transfected with 3′tRF-AlaAGC mimic demonstrated resistance to drugs and enhanced malignant cellular behavior. Simultaneously, the 3′tRF-AlaAGC mimic increased the expression of M2 macrophage markers IL-10 and CCL-22, and decreased the expression of M1 macrophage markers TNF-α and IL-1β. Conversely, the 3′tRF-AlaAGC inhibitor has the opposite effect. All above results revealed that 3′tRF-AlaAGC could regulate the phenotype of macrophages.

NF-κb is one of the best understood immune-related pathways due to the increasing research, which has been shown to play a role in apoptosis by regulating genes involved in cell death [41, 42]. Here we found that the expression of NF-κb signaling pathway in BC chemoresistance tissues was enhanced. What's more, enriched signaling pathways for target genes of 3′tRF-AlaAGC identified by KEGG pathway analysis, it was found that NF-κb signaling pathway is also one of them. TRADD has previously been shown to target the Micro-RNA-30c-2-3p in BC and negatively regulate NF-κb signaling [43]. In the present study, we showed that TRADD expression was positively associated with NF-κb by use of public database. Moreover, there are potential binding sites for TRADD on 3′tRF-AlaAGC, which could regulate TRADD expression in BC cells. On the other hand, RNA pull-down assay results evidenced that the association of 3′tRF-AlaAGC with TRADD. Interestingly, rescue experiments displayed that the suppression of TRADD

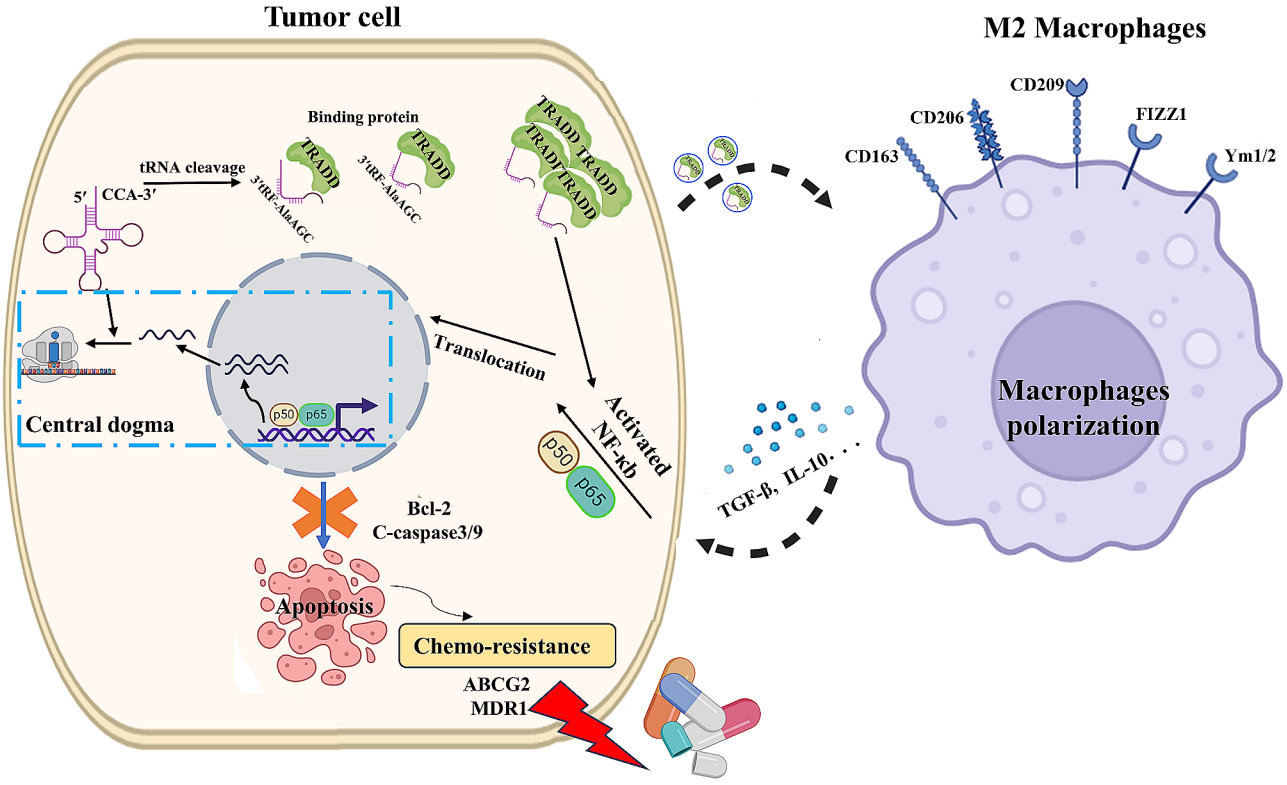

Fig. 9 Proposed working model 3′tRF-AlaAGC might modulate macrophage polarization via binding to TRADD and increase the effect of M2 macrophage on promoting the chemoresistance of BC cells through NF-κb signaling pathway

partially abolished the enhanced effect of 3′tRF-AlaAGC mimic on phenotype of M2 macrophages. And then, BC cells co-cultured with M2 macrophages transfected with 3′tRF-AlaAGC mimic showed stronger chemoresistance, cell proliferation and weaker apoptosis ability. Meanwhile, higher expression of ABCG2, Bcl-2 and lower expression of cleaved caspase-3 and cleaved caspase-9 in experimental group. Certainly, the expression of TARDD, p-65 and P-p-65 in MCF-7 cells co-cultured with M2 macrophages transfected with 3′tRF-AlaAGC mimic were significantly increased. Our results indicated that 3′tRF-AlaAGC in M2 macrophages regulate the chemoresistance BC cells via NF-κb signaling pathway. In the previous study showing the tRF-3022b modulates cell apoptosis and M2 macrophage polarization via binding to cytokines in colorectal cancer [44]. In ovarian cancer, miR-21 modulated the polarization of M2 macrophages and regulate the chemoresistance via PI3K/AKT signaling [45]. Therefore, we speculated that 3′tRF-AlaAGC might modulate macrophage polarization via binding to TRADD and increase the effect of M2 macrophage on promoting the chemoresistance of BC cells through NF-κb signaling pathway (Fig. 9).

Conclusion

In summary, we demonstrate, for the first time, 3′tRF-AlaAGC is specifically overexpressed in Adriamycin resistant BC cells and enhances drug resistance through NF-κb signaling pathway. In addition, 3′tRF-AlaAGC modulates M2 macrophage polarization by binding to TRADD.

Abbreviations

BC	Breast Cancer
tDRs	tRNA-Derived small RNAs
NF-κb	Nuclear Factor-κb
TRADD	Type 1-Associated Death Domain Protein
ADR	Adriamycin
ncRNAs	non-coding RNAs
TME	Tumor Microenvironment
PMA	Phorbol 12-myristate 13-acetate
LPS	Lipopolysaccharides
IL-4	Interleukin-4
IL-13	Interleukin-13
qRT-PCR	quantitative Real-Time PCR
GO	Gene Ontology
KEGG	Kyoto Encyclopedia Of Genes And Genes And Genome
BP	Biological Processes
CC	Cellular Components
MF	Molecular Functions
IC_{50}	Half-maximal Inhibitory Concentration
CCK-8	Cell Counting Kit-8
OD	Optical Density
FITC	Fluorescein Isothiocyanate
PI	Propidium Iodide
IHC	Immunohistochemistry

TUNEL	Terminal Deoxynucleotidyl Transferase-Mediated Dutp Nick End Labeling
ELISA	Enzyme-Linked Immunosorbent Assay
DAPI	4′,6-diamidino-2-phenylindole
ABCG2	ATP Binding Cassette Subfamily G Member 2
MDR1	Multi Drug Resistance 1
GEO	Gene Expression Omnibus
TAMs	Tumor Associated Macrophages

Supplementary Information

The online version contains supplementary material available at https://doi.org/10.1186/s12967-024-05513-z.

Supplementary Material 1

Acknowledgements
Not applicable.

Author contributions
(I)Conception and design: Dongping Mo, Xun Tang, Feng Yan; (II) Provision of study materials or patients: Yuyan Ma; Dayu Chen, (III) Collection and assembly of data: Weiguo Xu, Ning Jiang, Junyu Zheng; (IV) Data analysis and interpretation: Dongping Mo, Yuyan Ma, Xun Tang; (V) Manuscript writing and Obtaining funding: Dongping Mo, (VI)Supervision: Feng Yan; (VII)Final approval of manuscript: All authors. All authors contributed to the article and approved the submitted version.

Funding
This study was supported by the National Natural Science Foundation of China (NO. 82002225).

Data availability
The original contributions presented in this study are include in the article. Further inquiries can be directed to the corresponding author.

Declarations

Ethics approval and consent to participate
The studies involving human participants and animal experimental procedures were reviewed and approved by the Ethics Committee of Nanjing Medical University. The patients/participants provided their written informed consent to participate in this study.

Consent for publication
Not applicable.

Competing interests
The authors declare no potential conflicts of interest.

Author details
[1]Department of Clinical Laboratory, Nanjing Medical University Affiliated Cancer Hospital & Jiangsu Cancer Hospital & Jiangsu Institute of Cancer Research, Baizi Ting No.42, Nanjing 210009, China
[2]Department of General Surgery, Naning Medical University Affiliated Cancer Hospital & Jiangsu Cancer Hospital & Jiangsu Institute of Cancer Research, Baizi Ting No.42, Nanjing 210009, China
[3]Jiangsu Key Laboratory of Molecular and Translational Cancer Research, Baizi Ting No.42, Nanjing 210009, China

Received: 6 May 2024 / Accepted: 16 July 2024
Published online: 30 July 2024

References

1. Sung H, Ferlay J, Siegel RL et al. Global Cancer Statistics. 2020: GLOBOCAN Estimates of Incidence and Mortality Worldwide for 36 Cancers in 185 Countries. CA: a cancer journal for clinicians 2021, 71(3):209–249.
2. Christowitz C, Davis T, Isaacs A, et al. Mechanisms of doxorubicin-induced drug resistance and drug resistant tumour growth in a murine breast tumour model. BMC Cancer. 2019;19(1):757.
3. Mattioli R, Ilari A, Colotti B, et al. Doxorubicin and other anthracyclines in cancers: activity, chemoresistance and its overcoming. Mol Aspects Med. 2023;93:101205.
4. Jamialahmadi K, Zahedipour F, Karimi G. The role of microRNAs on doxorubicin drug resistance in breast cancer. J Pharm Pharmacol. 2021;73(8):997–1006.
5. Yao N, Fu Y, Chen L, et al. Long non-coding RNA NONHSAT101069 promotes epirubicin resistance, migration, and invasion of breast cancer cells through NONHSAT101069/miR-129-5p/Twist1 axis. Oncogene. 2019;38(47):7216–33.
6. Castaldo V, Minopoli M, Di Modugno F, et al. Upregulated expression of miR-4443 and miR-4488 in drug resistant melanomas promotes migratory and invasive phenotypes through downregulation of intermediate filament nestin. J Exp Clin Cancer Res. 2023;42(1):317.
7. Wu Q, Wang H, Liu L, et al. Hsa_circ_0001546 acts as a miRNA-421 sponge to inhibit the chemoresistance of gastric cancer cells via ATM/Chk2/p53-dependent pathway. Biochem Biophys Res Commun. 2020;521(2):303–9.
8. Pekarsky Y, Balatti V, Croce CM. tRNA-derived fragments (tRFs) in cancer. J Cell Commun Signal. 2023;17(1):47–54.
9. Mao M, Chen W, Huang X, et al. Role of tRNA-derived small RNAs(tsRNAs) in the diagnosis and treatment of malignant tumours. Cell Commun Signal. 2023;21(1):178.
10. Wang Y, Weng Q, Ge J, et al. tRNA-derived small RNAs: mechanisms and potential roles in cancers. Genes Dis. 2022;9(6):1431–42.
11. Zhang Y, Gu X, Li Y, et al. Multiple regulatory roles of the transfer RNA-derived small RNAs in cancers. Genes Dis. 2023;11(2):597–613. Published 2023 Apr 13.
12. Kim HK, Fuchs G, Wang S, et al. A transferRNA-derived small RNA regulates ribosome biogenesis. Nature. 2017;552(7683):57–62.
13. Wang L, Peng B, Yan Y, et al. The tRF-3024b hijacks mir-192-5p to increase BCL-2-mediated resistance to cytotoxic T lymphocytes in esophageal squamous cell carcinoma. Int Immunopharmacol. 2024;126:111135.
14. Sun C, Huang X, Li J, et al. Exosome-transmitted tRF-16-K8J7K1B promotes tamoxifen resistance by reducing Drug-Induced Cell apoptosis in breast Cancer. Cancers (Basel). 2023;15(3):899.
15. Barker HE, Paget JT, Khan AA, et al. The tumor microenvironment after radiotherapy:mechanisms of resistance and recurrence. Nat Rev Cancer. 2015;15(7):409–25.
16. Khalaf K, Hana D, Chou JT, et al. Aspects of the Tumor Microenvironment involved in Immune Resistance and Drug Resistance. Front Immunol. 2021;12:656364.
17. Ma H, Li YN, Song L, et al. Macrophages inhibit adipogenic differentiation of adipose tissue derived mesenchymal stem/stromal cells by producing pro-inflammatory cytokines. Cell Biosci. 2020;10:88.
18. Jang JH, Kim DH, Lim JM, et al. Breast Cancer Cell-Derived Soluble CD44 promotes Tumor Progression by triggering macrophage IL1beta production. Cancer Res. 2020;80(6):1342–56.
19. Sawa-Wejksza K, Kandefer-Szerszen M. Tumor-Associated macrophages as Target for Antitumor Therapy. Arch Immunol Ther Exp. 2018;66(2):97–111.
20. Shu Y, Qin M, Song Y, et al. M2 polarization of tumor-associated macrophages is dependent on integrin beta3 via peroxisome proliferator-activated receptor-gamma up-regulation in breast cancer. Immunology. 2020;160(4):345–56.
21. Zhou M, He X, Zhang J, et al. tRNA-derived small RNAs in human cancers: roles, mechanisms, and clinical application. Mol Cancer. 2024;23(1):76.
22. Yang M, Mo Y, Ren D, et al. Transfer RNA-derived small RNAs in tumor microenvironment. Mol Cancer. 2023;22(1):32.
23. Tao EW, Wang HL, Cheng WY, et al. A specific tRNA half, 5′tiRNA-His-GTG, responds to hypoxia via the HIF1α/ANG axis and promotes colorectal cancer progression by regulating LATS2. J Exp Clin Cancer Res. 2021;40(1):67.
24. Mitchell S, Vargas J, Hoffmann A. Signaling via the NFκB system. Wiley Interdiscip Rev Syst Biol Med. 2016;8(3):227–41.
25. Chen Y, Gu Y, Xiong X, et al. Roles of the adaptor protein tumor necrosis factor receptor type 1-associated death domain protein (TRADD) in human diseases. Biomed Pharmacother. 2022;153:113467.
26. Zhang N, Kisiswa L, Ramanujan A, et al. Structural basis of NF-κB signaling by the p75 neurotrophin receptor interaction with adaptor protein TRADD through their respective death domains. J Biol Chem. 2021;297(2):100916.
27. Panoutsopoulou K, Magkou P, Dreyer T, et al. tRNA-derived small RNA 3′U-tRF^{ValCAC} promotes tumour migration and early progression in ovarian cancer. Eur J Cancer. 2023;180:134–45.

28. Qin C, Chen ZH, Cao R, et al. A novel tiRNA-Gly-GCC-1 promotes progression of Urothelial Bladder Carcinoma and directly targets TLR4. Cancers (Basel). 2022;14(19):4555.
29. Zhang Y, Qian H, He J, et al. Mechanisms of tRNA-derived fragments and tRNA halves in cancer treatment resistance. Biomark Res. 2020;8:52.
30. Ivanov P, O'Day E, Emara MM, et al. G-quadruplex structures contribute to the neuroprotective effects of angiogenin-induced tRNA fragments. Proc Natl Acad Sci U S A. 2014;111(51):18201–6.
31. Zhang H, Mañán-Mejías PM, Miles HN, et al. DDX3X and stress granules: emerging players in Cancer and Drug Resistance. Cancers (Basel). 2024;16(6):1131.
32. Emara MM, Ivanov P, Hickman T, et al. Angiogenin-induced tRNA-derived stress-induced RNAs promote stress-induced stress granule assembly. J Biol Chem. 2010;285(14):10959–68.
33. Erin N, Grahovac J, Brozovic A, et al. Tumor microenvironment and epithelial mesenchymal transition as targets to overcome tumor multidrug resistance. Drug Resist Updat. 2020;53:100715.
34. Xu Y, Wang X, Liu L, et al. Role of macrophages in tumor progression and therapy (review). Int J Oncol. 2022;60(5):57.
35. Li Y, Chen Z, Han J, et al. Functional and therapeutic significance of Tumor-Associated macrophages in Colorectal Cancer. Front Oncol. 2022;12:781233.
36. Zhou L, Li J, Liao M, et al. LncRNA MIR155HG induces M2 macrophage polarization and drug resistance of colorectal cancer cells by regulating ANXA2. Cancer Immunol Immunother. 2022;71(5):1075–91.
37. Gordon S, Taylor PR. Monocyte and macrophage heterogeneity. Nat Rev Immunol. 2005;5(12):953–64.
38. Mantovani A, Sozzani S, Locati M, et al. Macrophage polarization: tumor-associated macrophages as a paradigm for polarized M2 mononuclear phagocytes. Trends Immunol. 2002;23(11):549–55.
39. Zhao S, Mi Y, Guan B et al. Tumor-derived exosomal miR-934 induces macrophage M2 polarization to promote liver metastasis of colorectal cancer [published correction appears in J Hematol Oncol. 2021;14(1):33. J Hematol Oncol. 2020;13(1):156.
40. Wang X, Hu Z. tRNA derived fragment tsRNA-14783 promotes M2 polarization of macrophages in keloid. Biochem Biophys Res Commun. 2022;636(Pt 2):119–27.
41. Dorrington MG, Fraser IDC. NF-κB Signaling in macrophages: Dynamics, Crosstalk, and Signal Integration. Front Immunol. 2019;10:705.
42. Sun B, Hu C, Yang Z, et al. Midkine promotes hepatocellular carcinoma metastasis by elevating anoikis resistance of circulating tumor cells. Oncotarget. 2017;8(20):32523–35.
43. Shukla K, Sharma AK, Ward A, et al. MicroRNA-30c-2-3p negatively regulates NF-κB signaling and cell cycle progression through downregulation of TRADD and CCNE1 in breast cancer. Mol Oncol. 2015;9(6):1106–19.
44. Lu S, Wei X, Tao L, et al. A novel tRNA-derived fragment tRF-3022b modulates cell apoptosis and M2 macrophage polarization via binding to cytokines in colorectal cancer. J Hematol Oncol. 2022;15(1):176.
45. An Y, Yang Q. MiR-21 modulates the polarization of macrophages and increases the effects of M2 macrophages on promoting the chemoresistance of ovarian cancer. Life Sci. 2020;242:117162.

Publisher's Note